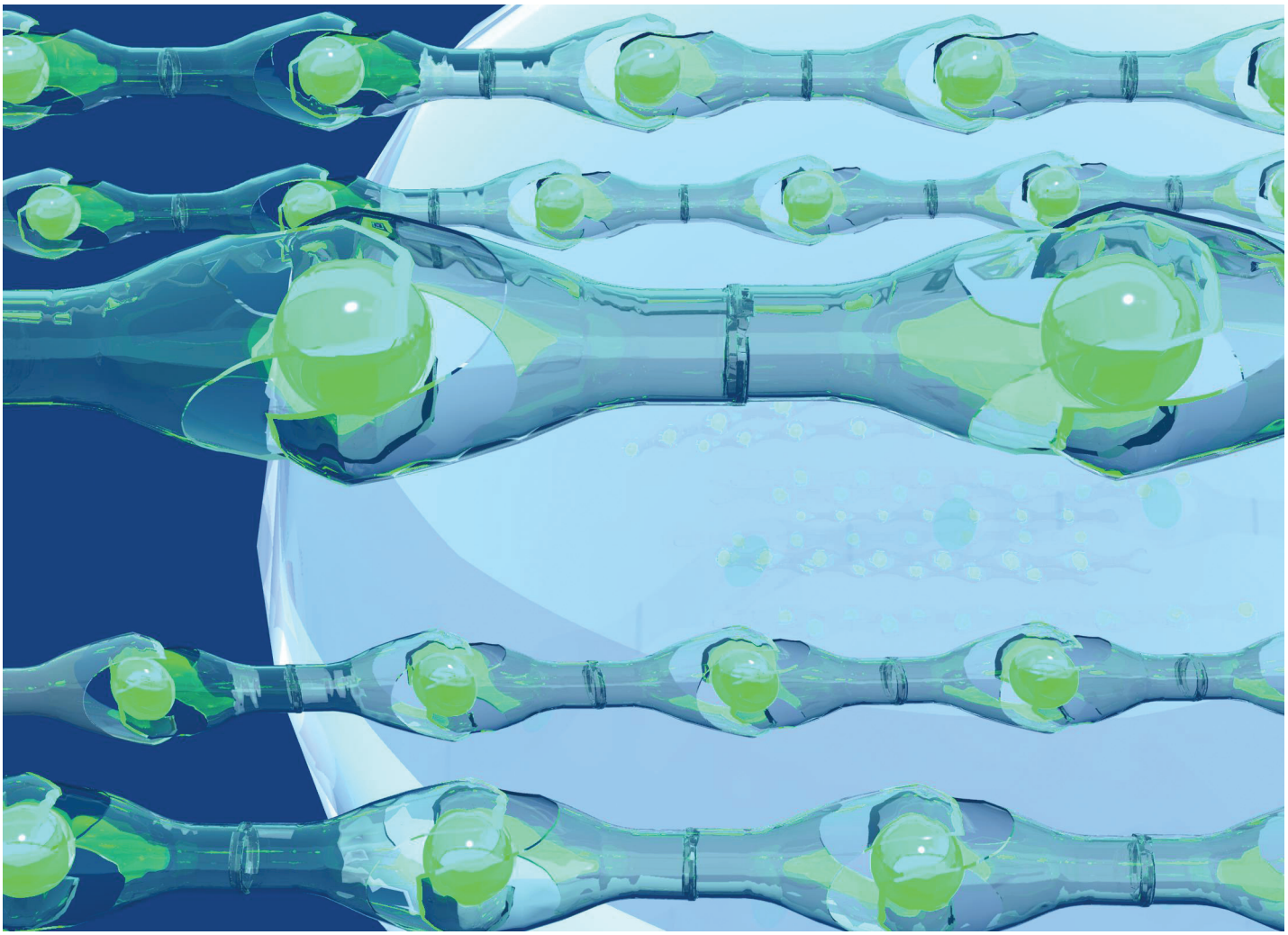

Showcasing research from Higuchi's group at National Institute for Materials Science, Japan.

Slow magnetic relaxation in a Tb(III)-based coordination polymer

A one-dimensional Tb-based coordination polymer (polyTb) was synthesized, which showed field-induced magnetic relaxation in solid and solution state as well as green luminescence due to f–f transition.

As featured in:

See Masayoshi Higuchi *et al.*, *Dalton Trans.*, 2018, **47**, 16066.

ROYAL SOCIETY OF CHEMISTRY

rsc.li/dalton

Registered charity number: 207890

Dalton Transactions

PAPER

View Article Online
View Journal | View Issue

Cite this: *Dalton Trans.*, 2018, **47**, 16066

Slow magnetic relaxation in a Tb(III)-based coordination polymer†

Takefumi Yoshida, [a] Yemineni S. L. V. Narayana,[a] Hitoshi Abe [b,c] and Masayoshi Higuchi *[a]

Received 31st July 2018,
Accepted 18th September 2018

DOI: 10.1039/c8dt03125h

rsc.li/dalton

A Tb(III)-based coordination polymer (**polyTb**) was synthesized by complexation of $Tb(NO_3)_3{\cdot}(6H_2O)$ and 4′,4‴′-[1,1′-biphenyl]-4,4′-diylbis[6,6″-bis(ethoxycarbonyl)2′:6′,2″-terpyridine](L). The polymer structure was determined by Job's plots, DFT calculation, and X-ray absorption fine structure (XAFS) measurement. Job's plots indicated that the mole ratio (Tb ion : L) is 1 : 1. The optimized model structures suggested a La model: the $LaN_6{\cdots}(O{=}C)_2$ model. The bond distances of La–O and La–N are ~2.80 Å and 2.60 Å, respectively. The EXAFS fitting indicated that the bond distances of Tb–O and Tb–N are 2.65 Å and 2.95 Å, respectively. **polyTb** shows field-induced magnetic relaxation in the solid and solution state. The luminescence of **polyTb**, originating from an f–f transition, was observed (ϕ = 6.9%). **polyTb** formed a porous structure on a Si substrate, whereas a fibrous complex structure was formed on glass. **polyTb** chains are orientated on glass, which were determined by XRD.

Introduction

Coordination polymers (CPs) have received much attention due to their luminescence,[1] electrochromism,[1c,2] and ion conductivity.[3] These properties greatly depend on the metal species included in the polymer. The zinc and lanthanoid polymers present good light emission properties. Holten-Andersen reported white-light-emitting lanthanoid metallogels with switching properties.[1d] Luminescent CPs will realize practical probes and sensors.

As for the magnetic properties, Kurth reported spincrossover phenomena.[4a] Murray reported light induced excited spin state trapping.[4b] A molecular magnet is one of the prime candidates for quantum memory since it can store information on spin such as up spin and down spin. Organic π-conjugated polymers with radicals show slow magnetic relaxation owing to magnetic ordering.[5] Although the reported polymer shows a larger magnetic moment, it is difficult to store the information on an independent spin centre because of an isotropic π-orbital. Since lanthanoid (Ln) ions have strong intrinsic magnetic anisotropy and large activation barriers (Δ) between up-spins and down-spins, as a result of spin–orbital interaction, the complexes will act as molecular magnets.[6] There are several lanthanoid compounds with a 1D chain structure, but they have high crystallinity and cannot be treated like soft materials.[6e–f] Molecular orientation is one of the important factors for making molecular-based optical devices or memory, because there is orientation dependence for properties that arise from molecular polarization or magnetic anisotropy. Successful research on molecular-based quantum devices has been reported, where the molecule attaches onto a surface by vacuum deposition or Langmuir–Blodgett film formation.[7] On the other hand, molecular-based bulk devices have been reported, where the molecule attaches onto the surface by simple coating.[8] CPs have good film forming abilities and can form composites of **polyTb** and other polymers.[9] This will extend the application of the CPs as molecular magnets and/or luminescent sensors. We synthesized a Tb(III)-base coordination polymer (**polyTb**) using a terpyridine ligand (L: 4′,4‴′-[1,1′-biphenyl]-4,4′-diylbis[6,6″-bis(ethoxycarbonyl) 2′:6′,2″-terpyridine], Fig. 1a) to reveal the expansivity of magnetic materials.

Results and discussion

First, we investigated the complexation behavior of Tb ions and L by Job's plots. A Job's plot at 340 nm is shown in Fig. 1b. The intensity at 340 nm gradually increases, when the

[a]*Electronic Functional Macromolecules Group, National Institute for Materials Science (NIMS), Tsukuba 305-0044, Japan. E-mail: HIGUCHI.Masayoshi@nims.go.jp*
[b]*Institute of Materials Structure Science High Energy Accelerator Research Organization (KEK) 1-1 Oho, Tsukuba, Ibaraki 305-0801, Japan*
[c]*Department of Materials Structure Science, School of High Energy Accelerator Science, SOKENDAI (the Graduate University for Advanced Studies) 1-1 Oho, Tsukuba, Ibaraki 305-0801, Japan*

†Electronic supplementary information (ESI) available. See DOI: 10.1039/c8dt03125h

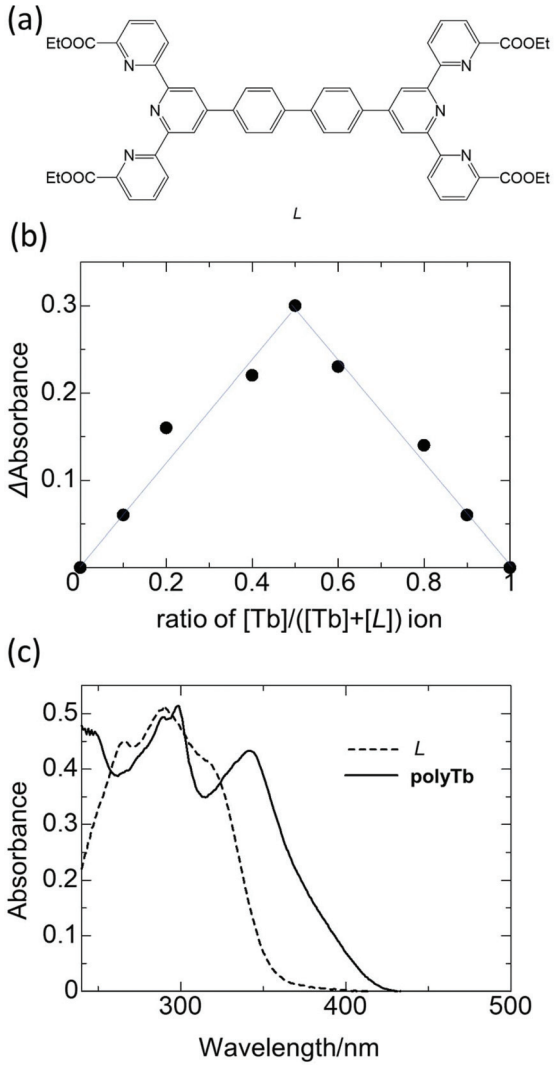

Fig. 1 (a) A structure of L; (b) Job's plots for the complexation of $Tb(NO_3)_3$ and L at 350 nm; (c) UV/vis spectrum of L and **polyTb**.

amount of Tb ion is increased up to 0.5. Then the intensity gradually decreases up to 1. These results indicated that the mole ratio is 1 : 1, or they formed a 1D chain structure (Fig. 2).

According to the results of Job's plots, we synthesized **polyTb** by 1 : 1 complexation of $Tb(NO_3)_3{\cdot}(6H_2O)$ and L. We described the synthesis of L in the Experimental section.

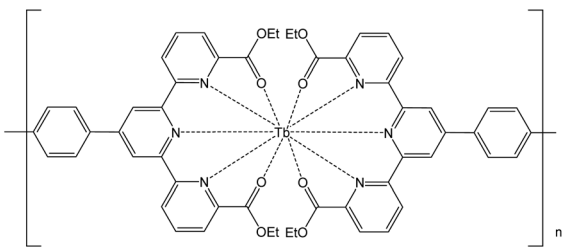

Fig. 2 An expected structure of **polyTb**.

Andreiadis reported the synthesis of a similar Eu complex of discrete small molecules by simple mixing of the metal salt and ligand in a solvent.[10] To L (9 mg, 0.01 mmol) was added $Tb(NO_3)_3{\cdot}6H_2O$ (4 mg, 0.01 mmol) in 20 ml CH_2Cl_2 solution. After several hours, a yellow solution of **polyTb** was obtained. After evaporation, we obtained a yellow solid of **polyTb**. **polyTb** was characterized by elemental analysis and IR spectra. The UV/vis spectra of **polyTb** and L are shown in Fig. 1c. There are π–π^* transition peaks of L at 250 nm 300 nm. There is a clear metal-to-ligand charge transition (MLCT) or ligand-to-metal charge transition (LNCT) peak of **polyTb** at 340 nm.

To estimate the coordination structure of **polyTb**, we made a La model: the $LaN_6{\cdots}(O{=}C)_2$ model instead of a Tb model (to avoid errors of calculation induced by multiple f^8 spins) and optimized the structures (Fig. 3). The optimized coordination structure of each model is shown in Fig. S1† (coordinates in Table S1†). The La ions have D_{4h}.[11] The bond distances of La–O and La–N are ~2.80 Å and 2.60 Å, respectively. These distances are similar to the reported coordination structure of the Eu complex with the terpyridine ligand which is an analogue of L, where there are an Eu–O bond (~2.44 Å) and an Eu–N bond (~2.68 Å).[10] Therefore, these models are appropriate for determining the coordination structure of **polyTb**. In addition, the intramolecular La–La distance was estimated to be more than 22 Å and the shortest intermolecular La–La distance was at least 11 Å (diameter of the ligand). Therefore, we concluded that there is no magnetic ordering among the Tb ions of **polyTb** due to long Tb–Tb distances.

For further evidence, we performed X-ray absorption fine structure measurements at the L_3-edge of the Tb ion at the Synchrotron Facility (BL-9A KEK). X-ray absorption near edge structures (XANES) at the Tb L_3-edge are shown in Fig. 4. The

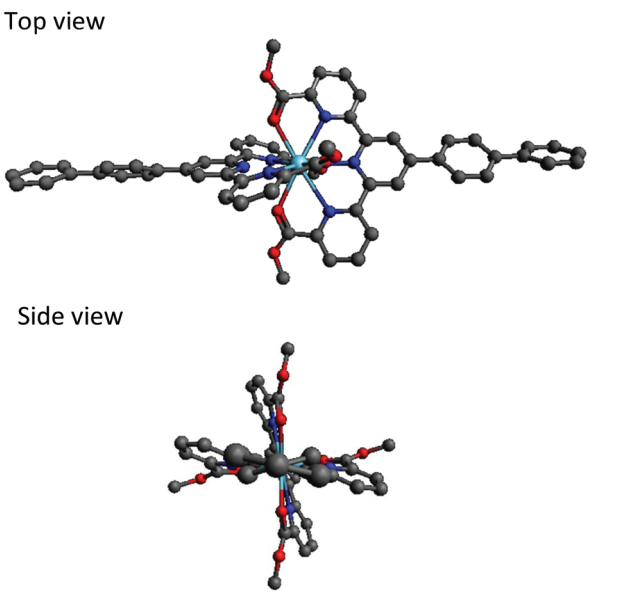

Fig. 3 The optimized structures of the La model. The ethoxycarbonyl groups were replaced with methoxycarbonyl groups for simplifying the calculation. Hydrogen atoms are omitted for clarity.

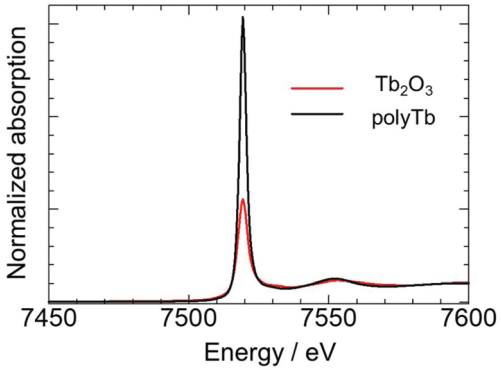

Fig. 4 XANES of Tb_2O_3 and **polyTb**.

Tb L_3-edge spectra of **1** was not shifted from 7519 eV (peak top of the edge of the standard sample of Tb_2O_3). The results indicate that the oxidation state of Tb ions of **1** is trivalent.[12] From the EXAFS region, the fitting revealed that the coordination bond lengths around the Tb ions (Tb–O, Tb–N) are 2.67 Å and 2.84 Å (R-factor; 1.5%, Table 1, EXAFS oscillation is shown in Fig. S2†). Both results relatively match to each model.

The χT *vs.* T plots for **polyTb** are shown in Fig. 5a (χ: magnetic susceptibility). The χT value for **polyTb** was constant at 10.5 cm^3 mol^{-1} K in the range of 100–300 K, consistent with the expected value for an uncoupled Tb ion (11.82 cm^3 mol^{-1} K). The values decreased with a decrease in temperature in the range of 10–100 K. These decrements were attributed to the depopulation of the m_J state of the Tb ion, and not to magnetic ordering. The reduced magnetization plots for **polyTb** almost overlapped each other, indicating that the magnetic anisotropy of **polyTb** is small (Fig. 5a inset). The magnetization *vs.* field plots for **polyTb** are shown in Fig. S3.† No hysteresis was observed.

No clear frequency dependence in zero dc field was observed for **polyTb**, because of a fast quantum tunneling relaxation process. However as soon as a dc field was applied, **polyTb** shows a clear frequency dependency of magnetic relaxation or slow magnetic relaxation, in which quantum tunneling is suppressed (Fig. 5b and S5†). Only a single relaxation time (τ) was obtained from the magnetic data acquired in a 3000 Oe field (although the τ values increase or the QTM is gradually suppressed up to 4000 Oe (Fig. S4†), we acquired the data using an applied field of 3000 Oe because of the maximum χ'' and symmetric relaxation curve) in the temperature range 2–4 K. Each relaxation was fitted using the Cole–Cole model.[13] All τ values are almost constant up to 4 K, a direct process ($\tau^{-1} = AH^4T$) or the Orbach process ($\tau^{-1} = \exp(-\Delta/k_BT)$) with a small Δ being dominant (Fig. S6†).

Table 1 Fitting results for Tb–O and Tb–N distances from EXAFS

	N	R (Å)	σ^2 (Å^2)	E_0 (eV)
Tb–O	4	2.83	0.025	−8.03
Tb–N	6	2.67	0.012	−8.03

N: coordination number, R: radius.

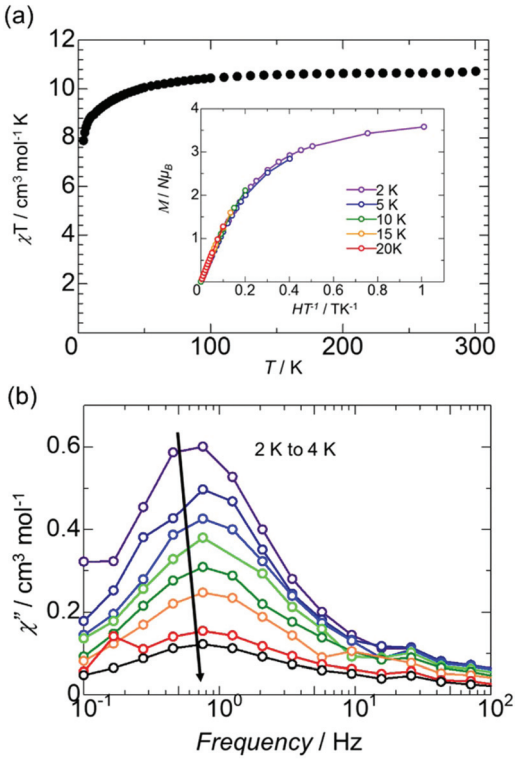

Fig. 5 (a) χT *vs.* T plots for **polyTb** measured under a field of 3000 Oe in the T range of 10–300 K. Inset: reduced magnetization of **polyTb** at various temperatures. (b) χ'' *vs.* T plots for **polyTb** under a field of 3000 Oe in the T range of 2–4 K.

Upon further investigation, we found that **polyTb** shows magnetic relaxation in the isolated state for making composites of **polyTb** and other polymers. We measured the AC susceptibility of a 1 mM CH_2Cl_2 solution of **polyTb**. There is magnetic relaxation which is faster than that in the solid-state (Fig. S7†). This is properly attributed to the coordination geometry change around the Tb ion that arises from the absence of stacking among the polymers, where the coordination environment around the Tb ion is less distorted. However, there is potential for composites of **polyTb** and other polymers showing magnetic properties under diluted conditions.

At room temperature (RT), upon excitation at 300 nm assigned to the π–π* transition of **polyTb**, the characteristic luminescence of the $^5D_4 \rightarrow {}^7F_n$ f–f transitions (n = 6, 5, 4, 3) of Tb ions was observed at 490, 542, 584, and 623 nm (Fig. 6). In addition, at 77 K, the characteristic luminescence of the f–f transitions of Tb ions was observed at 493, 543, 583, and 621 nm. The quantum yield of the region between 450 and 650 nm is 6.9% for the Tb f–f transition at RT. This low quantum yield is probably because of the high symmetry of the coordination sphere in the solution.[14] The excitation spectra of **polyTb** probed at 640 nm are shown in Fig. S8.† A

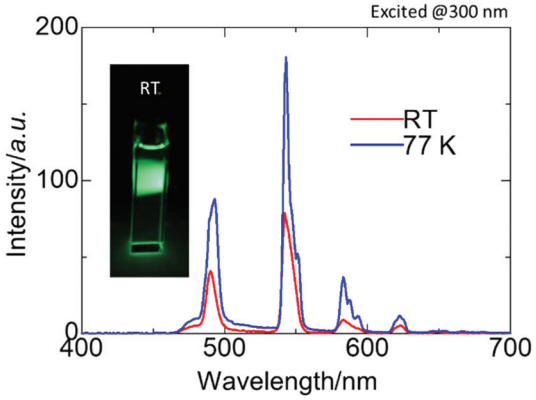

Fig. 6 Emission spectra of **polyTb** at RT and 77 K in $CHCl_3$ solution. Quantum yield was calculated as 6.9% at RT.

broad band with a peak at 300 nm was observed, where the shape of the edge is similar to that of the absorption spectra of **polyTb** in the range of 340–400 nm (corresponding to MLCT or LMCT: CT). This result indicated that the intra-molecular energy transfer terminated at the ^{1}CT band during irradiation. Then, energy transfer occurs in $^1\mathrm{CT} \rightarrow {}^3\mathrm{T}_1 \rightarrow {}^5\mathrm{D}_4$.

To investigate the film-forming properties of **polyTb**, we measured the morphology of **polyTb** on the surface by scanning electron microscopy (SEM), where we prepared a film by drop-casting. The SEM images of **polyTb** on Si and glass are shown in Fig. 7. **polyTb** formed a porous structure (diameter of the particle is about several 10 μm) on a Si substrate, whereas a fibrous complex structure (diameter of fibres is about several μm) was formed on glass. To investigate the difference of each surface, we performed X-ray diffraction (Fig. S9†). There are characteristic diffraction patterns, similar to the patterns of the powder sample, at 11.9, 12.5, 13.4, 15.8, 16.8 and 17.6 degrees on the Si substrate. There are also characteristic diffraction patterns at 11.9, 12.5, 13.4, 15.8, 16.8 and 17.6 degrees on the glass substrate. However, the peaks at 13.4 and 17.6 degrees are enhanced, whereas other peaks became weaker. These results indicated that **polyTb** formed random orientation on the Si substrate like powder and preferred orientation on the glass substrate. Although we couldn't index each peak because of low crystallinities, we expected that polymer chains along with the glass substrate, where peaks are correlated to inter-chain and/or inter-chain Tb–Tb distances, are enhanced. From the results of SEM and XRD, the polymer chains of **polyTb** properly formed an orientated fibrous structure along with the glass substrate by drop-casting. This is properly because polymer chains have a high affinity to glass. These properties enable the easy formation of polarized luminescence[7c] and orientated magnetic devices.[7a,b,8]

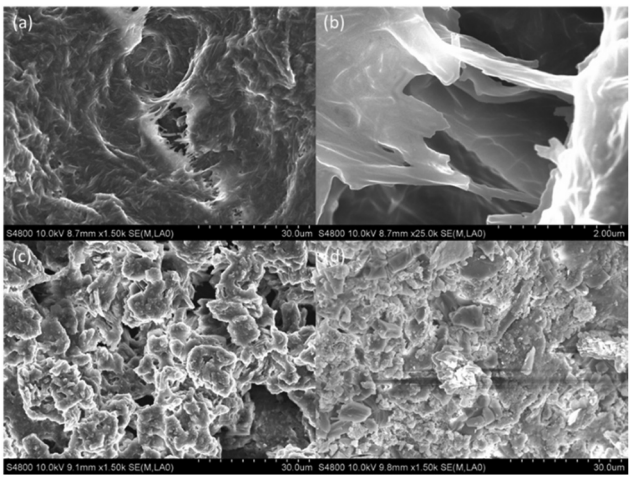

Fig. 7 SEM image of **polyTb** on (a,b) glass, (c) Si and (d) powder.

Conclusions

Among Tb-based CPs, **polyTb** was synthesized by complexation of $Tb(NO_3)_3{\cdot}(6H_2O)$ and L. The coordination structure (TbN_6O_4) is determined by Job's plots, DFT calculation, and X-ray absorption fine structure measurement; a 1D chain coordination polymer is formed. **polyTb** shows field-induced magnetic relaxation in the solid and solution state. The luminescence of **polyTb**, originating from an f–f transition, was observed (f = 6.9%). The coordination structure around Ln ions is the dominant factor for both magnetism and luminescence. However, it is hard to obtain information about the structure due to low crystallinity. In this work, we estimated the structure of CPs by DFT calculation and XAFS measurement. It is an effective method for designing high performance CPs which are molecular magnets. In addition, **polyTb** formed a porous structure on the Si substrate, whereas a fibrous complex structure was formed on glass. The **polyTb** film is orientated on glass, determined by XRD. In conclusion, we synthesized materials which show slow magnetic relaxation and orientation on the surface. These properties will simplify the fabrication of optical and magnetic devices.

Experimental

Synthesis of polyTb

To 40 mL of a DMSO solution of diethyl 4′-(4-bromophenyl)-[2,2′:6′,2″-terpyridine]-6,6″-dicarboxylate (0.30 g, 0.56 mmol) were added bis(pinacolato)diboron (0.157 g, 0.62 mmol), K_2CO_3 (0.39 g, 2.81 mmol), and $PdCl_2(PPh_3)_2$ (0.035 g, 0.56 mmol). The resultant reaction mixture was stirred at 100 °C under a nitrogen atmosphere for 12 h. After completion of the reaction, the solvent was removed under reduced pressure at 100 °C. The reaction mixture was cooled to room temperature and $CHCl_3$ (50 mL) was added. The catalyst was removed by filtration and washed thoroughly with $CHCl_3$. The filtrate was then washed with H_2O. The separated organic layer was dried over Na_2SO_4, filtered, concentrated, and purified by column chromatography on silica gel ($CHCl_3$/*n*-hexane =

90 : 10, then pure $CHCl_3$), and then finally purified by HPLC ($CHCl_3$) affording the desired product (L) (0.17 g, 33%) as a white solid. ^{1}H NMR (300 MHz, $CHCl_3$, 298 K) 8.94 (s, 4H), 8.88 (d, 4H), 8.18 (d, 4H), 8.04 (m, 8H), 7.90 (s, 4H), 4.51 (q, 8H), 1.49 (t, 12H), HR-MS: found *m*/*z*: 927.32 [M + Na]; $C_{54}H_{44}N_6O_8$ [M] requires 904.32. To L (9 mg, 0.01 mmol) was added $Tb(NO_3)_3{\cdot}6H_2O$ (4 mg, 0.01 mmol) in 20 ml CH_2Cl_2 solution. After several hours, a yellow solution of **polyTb** was obtained. After evaporation, we obtained a yellow solid of **polyTb**. Elemental analysis: Found: C, 45.49; H, 4.00; N, 9.07 Calc. for $[TbL](NO_3)_3{\cdot}(6H_2O + CH_2Cl_2) = C_{55}H_{58}N_9O_{23}Cl_2Tb$: C, 45.78; H, 4.05; N, 8.74%. IR spectrum (KBr, cm^{-1}): 3051 (m), 2999 (m), 1604 (s), 1628 (s), 1587 (s), 1567 (m), 1540 (m), 1469 (m), 1395 (s), 798 (m), 725 (m).

Calculation

Structural optimizations were performed on the Gaussian16 program package.[15] The molecular structure was determined using the model made by Avogadro.[16] The B3LYP[17] functional was used with the LanL2DZ basis set including the effective core potential.[18] The SCF procedure was performed under very strict conditions. An ultrafine integration grid was used for integration. Publication materials were visualized by Avogadro.[16]

XAFS measurement

X-ray absorption fine structure (XAFS) measurements were carried out at the BL9A beamline of the Photon Factory, the High Energy Accelerator Research Organization (KEK), under the proposal no. 2017PF-04. Structural analysis was performed on the Demeter software platform.[19] We used the optimized structure and reported crystal data[10] for calculating F_{eff}.

Spectroscopy

UV-vis spectra were acquired on a SHIMADZU UV-2550 UV-visible spectrophotometer. FT-IR spectra were acquired on a FTIR-8400S infrared spectrophotometer. Emission and excitation spectra were acquired in $CHCl_3$ solution on a SHIMADZU RF-5300PC spectrofluorophotometer with Oxford OptistatDN cryostats. The absolute emission quantum yields and emission lifetimes were measured on a Hamamatsu Photonics K. K. absolute PL quantum yield spectrometer 9920-02G.

Magnetometry

DC and AC magnetic susceptibility measurements were performed on a solid polycrystalline sample on a Quantum Design MPMS SQUID magnetometer under an applied dc field of 3000 Oe.

Conflicts of interest

There are no conflicts to declare.

Acknowledgements

This research is financially supported by the JST-CREST project (grant number: JPMJCR1533). This work was conducted at the AIST Nano-Processing Facility, supported by the "Nanotechnology Platform Program" of the Ministry of Education, Culture, Sports, Science and Technology (MEXT), Japan. The calculations in this study were performed on a Numerical Materials Simulator at NIMS. XAFS measurements were performed under the approval of PF-PAC No. 2017PF-04.

Notes and references

1 (*a*) D. Yang, Y. Wang, D. Liu, Z. Li and H. Li, *J. Mater. Chem. C*, 2018, **6**, 1944–1950; (*b*) R. Aoki, R. Toyoda, J. F. Kögel, R. Sakamoto, J. Kumar, Y. Kitagawa, K. Harano, T. Kawai and H. Nishihara, *J. Am. Chem. Soc.*, 2017, **139**, 16024–16027; (*c*) S. Pai, M. Moos, M. H. Schreck, C. Lambert and D. G. Kurth, *Inorg. Chem.*, 2017, **56**, 1418–1432; (*d*) P. Chen, Q. Li, S. Grindy and N. Holten-Andersen, *J. Am. Chem. Soc.*, 2015, **137**, 11590–11593; (*e*) R. Dobrawa and F. Würthner, *Chem. Commun.*, 2002, 1878–1879, DOI: 10.1039/B205478G; (*f*) S. C. Yu, C. C. Kwok, W. K. Chan and C. M. Che, *Adv. Mater.*, 2003, **15**, 1643–1647.

2 (*a*) S. Pai, M. Moos, M. H. Schreck, C. Lambert and D. G. Kurth, *Inorg. Chem.*, 2017, **56**, 1418–1432; (*b*) C. Chakraborty, R. K. Pandey, U. Rana, M. Kanao, S. Moriyama and M. Higuchi, *J. Mater. Chem. C*, 2016, **4**, 9428–9437.

3 R. K. Pandey, U. Rana, C. Chakraborty, S. Moriyama and M. Higuchi, *ACS Appl. Mater. Interfaces*, 2016, **8**, 13526–13531.

4 (*a*) Y. Bodenthin, G. Schwarz, Z. Tomkowicz, T. Geue, W. Haase, U. Pietsch and D. G. Kurth, *J. Am. Chem. Soc.*, 2009, **131**, 2934–2941; (*b*) T. M. Ross, B. Moubaraki, D. R. Turner, G. J. Halder, G. Chastanet, S. M. Neville, J. D. Cashion, J. F. Létard, S. R. Batten and K. S. Murray, *Eur. J. Inorg. Chem.*, 2011, **2011**, 1395–1417.

5 (*a*) A. Rajca, J. Wongsriratanakul and S. Rajca, *Science*, 2001, **294**, 1503–1505; (*b*) N. A. Zaidi, S. R. Giblin, I. Terry and A. P. Monkman, *Polymer*, 2004, **45**, 5683–5689.

6 (*a*) T. P. Latendresse, V. Vieru, B. O. Wilkins, N. S. Bhuvanesh, L. F. Chibotaru and M. Nippe, *Angew. Chem., Int. Ed.*, 2018, **57**, 8164–8169; (*b*) M. Perfetti, M. A. Sørensen, U. B. Hansen, H. Bamberger, S. Lenz, P. P. Hallmen, T. Fennell, G. G. Simeoni, A. Arauzo, J. Bartolomé, E. Bartolomé, K. Lefmann, H. Weihe, J. Slageren and J. Bendix, *Adv. Funct. Mater.*, 2018, 1801846; (*c*) K. Katoh, S. Yamashita, N. Yasuda, Y. Kitagawa, B. K. Breedlove, Y. Nakazawa and M. Yamashita, *Angew. Chem., Int. Ed.*, 2018, **57**, 9262–9267; (*d*) J. Goura, E. Colacio, J. M. Herrera, E. A. Suturina, I. Kuprov, Y. Lan, W. Wernsdorfer and V. Chandrasekhar, *Chem. – Eur. J.*, 2017, **23**, 16621–16636; (*e*) E. Bartolomé, J. Bartolomé, A. Arauzo, J. Luzón, R. Cases, S. Fuertes, V. Sicilia,

A. I. Sánchez-Cano, J. Aporta, S. Melnic, D. Prodius and S. Shova, *J. Mater. Chem. C*, 2018, **6**, 5286–5299; (*f*) H.-L. Tsai, C.-I. Yang, W. Wernsdorfer, S.-H. Huang, S.-Y. Jhan, M.-H. Liu and G.-H. Lee, *Inorg. Chem.*, 2012, **51**, 13171–13180.

7 (*a*) H. Imada, K. Miwa, M. Imai-Imada, S. Kawahara, K. Kimura and Y. Kim, *Phys. Rev. Lett.*, 2017, **119**, 013901; (*b*) E. Moreno Pineda, T. Komeda, K. Katoh, M. Yamashita and M. Ruben, *Dalton Trans.*, 2016, **45**, 18417–18433; (*c*) M. Hasegawa, S. Kunisaki, H. Ohtsu and F. Werner, *Monatsh. Chem.*, 2009, **140**, 751–763.

8 I. Osaka, M. Saito, T. Koganezawa and K. Takimiya, *Adv. Mater.*, 2014, **26**, 331–338.

9 (*a*) D. G. Kurth, J. Pitarch López and W.-F. Dong, *Chem. Commun.*, 2005, 2119–2121; (*b*) D. G. Kurth, F. Caruso and C. Schüler, *Chem. Commun.*, 1999, 1579–1580.

10 E. S. Andreiadis, R. Demadrille, D. Imbert, J. Pécaut and M. Mazzanti, *Chem. – Eur. J.*, 2009, **15**, 9458–9476.

11 (*a*) S. Alvarez, P. Alemany, D. Casanova, J. Cirera, M. Llunell and D. Avnir, *Coord. Chem. Rev.*, 2005, **249**, 1693–1708; (*b*) A. Ruiz-Martínez, D. Casanova and S. Alvarez, *Chem. – Eur. J.*, 2008, **14**, 1291–1303.

12 A. Potdevin, G. Chadeyron, V. Briois, F. Leroux and R. Mahiou, *Dalton Trans.*, 2010, **39**, 8718–8724.

13 K. S. Cole and H. Robert, *J. Chem. Phys.*, 1941, **9**, 341.

14 Y. Hasegawa, M. Yamamuro, Y. Wada, N. Kanehisa, Y. Kai and S. Yanagida, *J. Phys. Chem. A*, 2003, **107**, 1697–1702.

15 M. J. Frisch, G. W. Trucks, H. B. Schlegel, G. E. Scuseria, M. A. Robb, J. R. Cheeseman, G. Scalmani, V. Barone, G. A. Petersson, H. Nakatsuji, X. Li, M. Caricato, A. V. Marenich, J. Bloino, B. G. Janesko, R. Gomperts, B. Mennucci, H. P. Hratchian, J. V. Ortiz, A. F. Izmaylov, J. L. Sonnenberg, D. Williams-Young, F. Ding, F. Lipparini, F. Egidi, J. Goings, B. Peng, A. Petrone, T. Henderson, D. Ranasinghe, V. G. Zakrzewski, J. Gao, N. Rega, G. Zheng, W. Liang, M. Hada, M. Ehara, K. Toyota, R. Fukuda, J. Hasegawa, M. Ishida, T. Nakajima, Y. Honda, O. Kitao, H. Nakai, T. Vreven, K. Throssell, J. A. Montgomery Jr., J. E. Peralta, F. Ogliaro, M. J. Bearpark, J. J. Heyd, E. N. Brothers, K. N. Kudin, V. N. Staroverov, T. A. Keith, R. Kobayashi, J. Normand, K. Raghavachari, A. P. Rendell, J. C. Burant, S. S. Iyengar, J. Tomasi, M. Cossi, J. M. Millam, M. Klene, C. Adamo, R. Cammi, J. W. Ochterski, R. L. Martin, K. Morokuma, O. Farkas, J. B. Foresman and D. J. Fox, *Gaussian16 (Revision B.01)*, Gaussian, Inc., Wallingford CT, 2016.

16 M. D. Hanwell, D. E. Curtis, D. C. Lonie, T. Vandermeersch, E. Zurek and G. R. Hutchison, *J. Cheminf.*, 2012, **4**, 17.

17 (*a*) A. D. Becke, *J. Chem. Phys.*, 1993, **98**, 5648–5652; (*b*) C. Lee, W. Yang and R. G. Parr, *Phys. Rev. B: Condens. Matter Mater. Phys.*, 1988, **37**, 785–789.

18 (*a*) T. H. Dunning Jr. and P. J. Hay, *Modern Theoretical Chemistry*, ed. H. F. Schaefer III, Plenum, New York, Vol. 3, 1977; (*b*) P. J. Hay and W. R. Wadt, *J. Chem. Phys.*, 1985, **82**, 270–283.

19 B. Ravel and M. Newville, *J. Synchrotron Radiat.*, 2005, **12**, 537–541.